Int. J. Heat Mass Transfer. Vol. 30, No. 5, pp. 855–868, 1987
Printed in Great Britain

0017-9310/87 $3.00+0.00

Natural convection in a shallow porous cavity—the Brinkman model

ASOK K. SEN

Department of Mathematical Sciences, Purdue University School of Science, P.O. Box 647, Indianapolis, IN 46223, U.S.A.

(*Received* 19 *November* 1985 *and in final form* 26 *August* 1986)

Abstract—The natural convection in a shallow porous rectangular cavity with differentially heated sidewalls is examined using the Brinkman model. The heat transfer rate through the cavity is determined in terms of a Nusselt number, in the limit of vanishingly small aspect ratio. Two types of boundary conditions are considered. Case I deals with a cavity with all rigid boundaries so that the no-slip boundary conditions can be imposed. In case II, the cavity has a free upper surface. The present analysis shows that the Brinkman model and Darcy's law give virtually the same result for the heat transfer rate when the Darcy number, based on the depth of the cavity, is less than the order of 10^{-4}. We also find that the presence of a free surface can significantly increase the heat transfer rate through the cavity, especially when the permeability of the medium is high.

1. INTRODUCTION

NATURAL convection in porous media is known to be important in a wide variety of engineering applications such as geothermal reservoirs, thermal insulation by fibrous materials, packed-bed catalytic reactors, underground spreading of chemical wastes and other pollutants, and the cooling of rotating superconducting machinery [1–4]. The many possible configurations in which the flow and heat transfer processes in such systems have been examined include a rectangular enclosure with differentially heated vertical sidewalls, an annular cavity with radial heating and an infinitely long horizontal porous layer heated from below. In most of these studies, Darcy's law which is empirically given by

$$\frac{\mu}{K}\mathbf{v} = -(\nabla p + \rho g\mathbf{k}) \tag{1}$$

is used as the momentum equation for the fluid. Darcy's law is found to give satisfactory results for flow velocities and heat transfer rate when the porous medium is closely packed, i.e. it has a low permeability. If, on the other hand, the porous medium consists of a sparse distribution of particles, as is often the case, e.g. in petroleum reservoirs, Darcy's law becomes inadequate since the presence of large void spaces within the medium gives rise to viscous shear in addition to the usual Darcy resistance. Due to the fact that high-porosity materials are becoming increasingly important in modern technological applications, it is essential to develop a clear understanding of the flow and heat transfer processes in such media.

From a mathematical viewpoint, Darcy's law leads to a differential equation which is of order one less than the Navier–Stokes equations. Therefore it cannot be used to satisfy all the boundary conditions in a given problem. Specifically, the conditions of impenetration and no-slip at a solid boundary and conditions between a porous medium and a clear fluid cannot be completely satisfied. Nevertheless, because of its inherent simplicity, many forms of modified boundary conditions, though somewhat artificial, have been improvized and used in conjunction with Darcy's law yielding physically meaningful results [5, 6]. An alternate and more appropriate approach was proposed by Brinkman [7] who extended the Darcy model by adding a viscous-like term in equation (1) thereby making it a second-order equation. This extended-Darcy equation which can be written in the form

$$\frac{\mu}{K}\mathbf{v} = -(\nabla p + \rho g\mathbf{k}) + \mu'\nabla^2\mathbf{v} \tag{2}$$

has become known as the Brinkman equation. A rigorous theoretical justification of equation (2) has been given by Tam [8] and Lundgren [9], among others. The Brinkman equation removes the deficiencies of Darcy's law in the sense that it is applicable to media with high permeability and can account for all the boundary conditions at a solid surface or a fluid interface. Although the effective viscosity μ' appearing in equation (2) was recently shown [10] to be less than μ, the pore fluid value, it has been a common practice to take these two viscosities to be equal [11, 12]. The purpose of the present paper is to examine the effect of a solid boundary and a free surface on the rate of heat transfer through a rectangular porous cavity using the Brinkman model.

The first theoretical investigation of natural convection in a porous enclosure by the use of the Brinkman model was made by Chan *et al.* [13] who studied the flow and heat transfer rate in a rectangular box with solid (impermeable) walls. The box is differentially

NOMENCLATURE

A	aspect ratio of cavity, d/l
A^*, B^*, C^*, D^*	constants in the core streamfunction (15a)
C_p	specific heat of liquid
Da	Darcy number, K/d^2
d	depth of cavity
Gr	Grashof number
g	acceleration due to gravity
K	permeability of the porous medium
$\mathbf{k}$	unit vector pointed vertically upward
k_1	horizontal temperature gradient in the core region, expression (15b)
k_2	constant in expression (15b) for the core temperature
l	width of cavity
M	integral given by equation (45)
Nu	Nusselt number
Pr	Prandtl number
p	pressure
Ra	Rayleigh number
T	temperature
u	horizontal velocity component
u_*	characteristic velocity
v	vertical velocity component
$\mathbf{v}$	velocity vector
x	horizontal distance variable
y	vertical distance variable.

Greek symbols

α	effective thermal diffusivity of the porous medium
β	coefficient of thermal expansion of the liquid
η	horizontal distance variable in the boundary layer region adjacent to the cold sidewall
λ_l	thermal conductivity of the liquid
λ_s	thermal conductivity of the solid matrix
λ	effective thermal conductivity, $\lambda_l + (1-\phi)\lambda_s$
μ	viscosity of the liquid
μ'	effective viscosity
ν	kinematic viscosity of the liquid
ξ	horizontal distance variable in the boundary layer region adjacent to the hot sidewall
ρ	density of the liquid
σ	dimensionless Darcy parameter, $Da^{-1/2}$
ϕ	porosity
ψ	streamfunction.

heated in the horizontal direction. Chan *et al.* [13] considered enclosures with aspect ratios (depth/width) greater than or equal to one. Their numerical computations indicate that when the Darcy number based on the width of the enclosure is less than 10^{-3}, Darcy's law and the Brinkman equation give virtually the same result for the heat transfer rate. Within the past few years there has been a renewed interest in the use of the Brinkman equation for analyzing flows through porous media. Rudraiah *et al.* [14] used this model to investigate convective instabilities of a fluid-saturated porous layer heated from below. In a different context, the Brinkman equation is used by Nandakumar and Masliyah [15] to determine the flow of a Newtonian fluid past a permeable sphere and by Haber and Mauri [16] in their study of flow around a porous sphere with a solid core. More recently, Tong and Subramanian [17] examined the boundary layer regime for natural convection in a Brinkman medium inside enclosures with an aspect ratio of $O(1)$. To the author's knowledge, no analysis has yet appeared dealing with the problem of natural convection in a shallow porous cavity using the Brinkman model. The main purpose of this paper is to present such an analysis.

Several investigators [18] analyzed this shallow cavity problem using Darcy's law. Among them, Hickox and Gartling [19] applied the Galerkin form of the finite element method and numerically computed the heat transfer rate through the cavity in terms of a Nusselt number. Approximate analytical expressions for the Nusselt number have been derived by Walker and Homsy [20] and Bejan and Tien [21]. A comparison of the heat transfer results obtained from the present study and from those using Darcy's law will be made in Section 7.

In the original form, neither Darcy's law, equation (1), nor the Brinkman equation, equation (2), incorporates inertial effects. Muskat [22] accounted for fluid inertia by introducing a velocity-squared term in the equation. Among others, Whitaker [23] and Slattery [24] and more recently Vafai and Tien [25] developed equations for fluid motion through a porous medium, including inertial effects. For the present purpose, we shall use the term $\mathbf{v}\cdot\nabla\mathbf{v}$ in equation (2) to represent the inertia forces, as did Rudraiah *et al.* [14]. We shall see, however, that under the assumptions the present analysis is carried out, the effects of inertia can actually be ignored.

Our analysis proceeds as follows. First, we examine buoyancy-driven convection in a shallow porous cavity with all rigid boundaries (case I). Our mathematical treatment parallels that of Cormack *et al.* [26] (who considered natural convection in a shallow cavity filled with a Newtonian liquid) and is based on the asymptotic limit that the aspect ratio of the cavity goes to zero ($A \to 0$). This is followed by an analysis of natural convection in a shallow porous

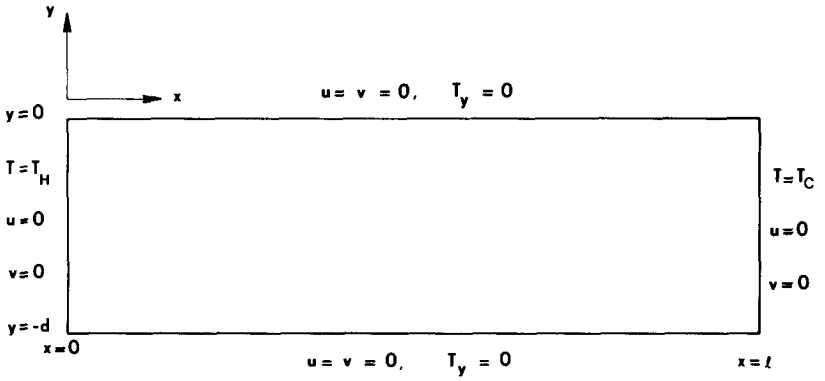

FIG. 1. Schematic diagram of the rectangular porous cavity with all rigid boundaries (case I).

cavity with a free upper surface (case II). The primary objective is to determine the heat transfer rate through the cavity in terms of a Nusselt number, correct to $O(A^3)$.

2. MATHEMATICAL FORMULATION

Consider a rectangular cavity of width l and depth d, as shown in Fig. 1. It is filled with a homogeneous, isotropic porous medium which consists of a sparse distribution of solid particles surrounded by a Newtonian liquid. The vertical sidewalls at $x = 0$, l are maintained at temperatures T_H and T_C, respectively, with $T_H > T_C$; the upper and lower surfaces are thermally insulated. In this section we consider case I only. For this case both the vertical and the horizontal boundaries of the cavity are assumed to be rigid so that the conditions of impenetration and no-slip can be imposed on these boundaries.

Under the Boussinesq approximation, the steady motion of the liquid inside the cavity can be described by the equations

$$u_x + v_y = 0 \tag{3a}$$

$$\rho(uu_x + vu_y) + \frac{\mu}{K}u = -p_x + \mu(u_{xx} + u_{yy}) \tag{3b}$$

$$\rho(uv_x + vv_y) + \frac{\mu}{K}v = -p_y + \mu(v_{xx} + v_{yy}) + \rho g\beta(T - T_C) \tag{3c}$$

$$\rho C_p(uT_x + vT_y) = \lambda(T_{xx} + T_{yy}) \tag{3d}$$

and the boundary conditions

$$x = 0: \quad u = v = 0, \quad T = T_H; \tag{4a}$$

$$x = l: \quad u = v = 0, \quad T = T_C; \tag{4b}$$

$$y = 0, -d: \quad u = v = 0, \quad T_y = 0. \tag{4c}$$

These equations and the boundary conditions are nondimensionalized by introducing the following primed variables

$$x = lx', \quad y = dy', \quad u = u_* u', \quad v = Au_* v',$$
$$p = (\mu u_* l/K)p', \quad T = T_C + (T_H - T_C)T'. \tag{5}$$

Here the characteristic velocity is chosen to be

$$u_* = AKg\beta(T_H - T_C)/\nu. \tag{6}$$

Rewriting equations (3) in terms of the primed variables by the use of equations (5) and subsequently dropping the primes, we arrive at the following system of dimensionless equations

$$u_x + v_y = 0 \tag{7a}$$

$$Gr\,A^2(uu_x + vu_y) + u = -p_x + Da(A^2u_{xx} + u_{yy}) \tag{7b}$$

$$Gr\,A^4(uv_x + vv_y) + A^2v = -p_y + Da\,A^2(A^2v_{xx} + v_{yy}) + T \tag{7c}$$

$$Ra\,A^2(uT_x + vT_y) = A^2T_{xx} + T_{yy}. \tag{7d}$$

The dimensionless parameters, namely the Grashof number, the Rayleigh number and the Darcy number have the definitions

$$Gr = K^2g\beta(T_H - T_C)/(d\nu^2) \tag{8a}$$

$$Ra = Kg\beta d(T_H - T_C)/(\nu\alpha) \tag{8b}$$

$$Da = K/d^2. \tag{8c}$$

The quantity α appearing in equation (8b) is the effective thermal diffusivity; $\alpha = \lambda/\rho C_p$. Note that our definition of Darcy number is based on the depth of the cavity. There is a simple relationship among these three parameters. We have

$$Ra = Da^{-1}\,Gr\,Pr \tag{9}$$

where $Pr = \nu/\alpha$ is the Prandtl number.

The dimensionless forms of boundary conditions (4) are

$$x = 0: \quad u = v = 0, \quad T = 1; \tag{10a}$$

$$x = 1: \quad u = v = 0, \quad T = 0; \tag{10b}$$

$$y = 0, -1: \quad u = v = 0, \quad T_y = 0. \tag{10c}$$

It is convenient to introduce a streamfunction ψ such that

$$u = \psi_y, \quad v = -\psi_x \tag{11}$$

and eliminate the pressure from the momentum equations (7b) and (7c) by cross differentiation. The result is

$$Gr\,A^2[(\psi_y\psi_{xyy} - \psi_x\psi_{yyy}) + A^2(\psi_y\psi_{xxx} - \psi_x\psi_{xxy})] + A^2\psi_{xx} + \psi_{yy} = Da[\psi_{yyyy} + 2A^2\psi_{xxyy} + A^4\psi_{xxxx}] - T_x. \tag{12}$$

We may therefore deal with equations (12) and (7d) directly. Boundary conditions (10) can be replaced by the following conditions

$$x = 0: \quad \psi = \psi_x = 0, \quad T = 1; \tag{13a}$$

$$x = 1: \quad \psi = \psi_x = 0, \quad T = 0; \tag{13b}$$

$$y = 0, -1: \quad \psi = \psi_y = 0, \quad T_y = 0. \tag{13c}$$

As mentioned in the introduction, we consider that the cavity has a small aspect ratio ($A \ll 1$). In other words, we examine the problem given by equations (7d), (12) and (13), in the asymptotic limit $A \to 0$. In this limit, the flow field can be divided into two distinct regions: an outer (core) region away from the sidewalls where the flow is essentially horizontal, and an inner (boundary layer) region near each sidewall where the flow turns around and recirculates. The complete flow structure is obtained by determining the flows in the inner and outer regions separately and then joining them by means of an asymptotic matching procedure. The heat transfer rate through the cavity can be expressed in terms of a Nusselt number defined by

$$Nu = -\int_{-1}^{0} T_x\Big|_{x=1} \mathrm{d}y \tag{14}$$

which represents the dimensionless heat flux across the cold sidewall. Our aim is to compute the Nusselt number for both cases I and II, correct to $O(A^3)$. The present analysis is based on the assumption that the dimensionless parameters Da, Gr and Ra are all of $O(1)$.

3. THE CORE FLOW

It can be easily shown that in the limit $A \to 0$, the problem consisting of equations (7d) and (12) and boundary conditions (13) admits a parallel flow solution, away from the sidewalls. This core solution may be expressed as

$$\psi = k_1\left(A^*\mathrm{e}^{\sigma y} + B^*\mathrm{e}^{-\sigma y} + \frac{1}{2}y^2 + C^*y + D^*\right) \tag{15a}$$

$$T = -k_1x + k_2 - A^2k_1^2\,Ra\left(\frac{A^*}{\sigma}\mathrm{e}^{\sigma y} - \frac{B^*}{\sigma}\mathrm{e}^{-\sigma y} + \frac{1}{6}y^3 + \frac{C^*}{2}y^2 + D^*y\right) \tag{15b}$$

with

$$A^* = -1/[2\sigma(1 - \mathrm{e}^{-\sigma})] \tag{15c}$$

$$B^* = -1/[2\sigma(\mathrm{e}^{\sigma} - 1)] \tag{15d}$$

$$C^* = 1/2 \tag{15e}$$

$$D^* = (\mathrm{e}^{\sigma} + 1)/[2\sigma(\mathrm{e}^{\sigma} - 1)] \tag{15f}$$

and

$$\sigma = Da^{-1/2}. \tag{15g}$$

The integration constants k_1 and k_2 which may, in general, depend on A, Gr, Ra and σ can be determined by matching the core flow solutions, equations (15), with the turning flows near the sidewalls. Note however that k_1 and k_2 can be related by invoking the so-called centro-symmetry condition, i.e. by using the fact that the streamlines and the isotherms must be symmetric about the center of the cavity. In particular, we may write

$$T(1/2, -1/2) = 1/2. \tag{16}$$

Then equation (15b) gives

$$k_2 = \frac{1}{2}(1 + k_1) + A^2k_1^2\,Ra\left(\frac{A^*}{\sigma}\mathrm{e}^{-\sigma/2} - \frac{B^*}{\sigma}\mathrm{e}^{\sigma/2} - \frac{D^*}{2} + \frac{1}{24}\right). \tag{17}$$

Constant k_1 is now expanded in the form

$$k_1 = C_0 + C_1A + C_2A^2 + C_3A^3 + \ldots \tag{18}$$

where the new constants C_i ($i = 0, 1, 2, 3, \ldots$) may depend on Ra, Gr and σ. We shall see that in order to derive the Nusselt number up to $O(A^3)$, we need to evaluate the constants C_0, C_1, C_2 and C_3 only. For the determination of these constants, we now proceed to examine the turning flow regions near the sidewalls.

4. BOUNDARY LAYER FLOWS NEAR THE SIDEWALLS

In view of symmetry, it is sufficient to consider the boundary layer near one of the sidewalls. For definiteness, we analyze the turning flow in the region adjacent to the hot sidewall at $x = 0$ by introducing a stretched coordinate ξ such that

$$x = A\xi. \tag{19}$$

(The y-coordinate is left unstretched.) In these coordinates, equations (12) and (7d) become

$$\nabla^4\psi - \sigma^2\nabla^2\psi = A^{-1}\sigma^2 T_\xi + Gr\,A\sigma^2[\psi_y(\psi_{\xi yy} + \psi_{\xi\xi\xi}) - \psi_\xi(\psi_{yyy} + \psi_{\xi\xi y})] \quad (20a)$$

$$\nabla^2 T = Ra\,A(\psi_y T_\xi - \psi_\xi T_y) \quad (20b)$$

where ∇^2 and ∇^4 denote the Laplacian and biharmonic operators, respectively, with

$$\nabla^2 = \frac{\partial^2}{\partial\xi^2} + \frac{\partial^2}{\partial y^2}. \quad (21)$$

Boundary conditions (13a) and (13c) lead to

$$\xi = 0: \quad \psi = \psi_\xi = 0, \quad T = 1; \quad (22a)$$

$$y = 0, -1: \quad \psi = \psi_y = 0, \quad T_y = 0. \quad (22b)$$

These boundary conditions must be augmented by a set of matching conditions which are derived from the requirement that, for continuity in the flow structure, the flows in the core and the boundary layers must be smoothly connected. It follows that

$$\lim_{\xi\to\infty} \psi^{\mathrm{B}} = \lim_{x\to 0} \psi^{\mathrm{C}} \quad (23a)$$

and

$$\lim_{\xi\to\infty} T^{\mathrm{B}} = \lim_{x\to 0} T^{\mathrm{C}}. \quad (23b)$$

Superscripts B and C refer to the boundary layer and the core region, respectively. We now write the inner expansions

$$\psi = \tilde{\psi}_0(\xi, y) + A\tilde{\psi}_1(\xi, y) + A^2\tilde{\psi}_2(\xi, y) + A^3\tilde{\psi}_3(\xi, y) + \ldots \quad (24a)$$

$$T = \tilde{T}_0(\xi, y) + A\tilde{T}_1(\xi, y) + A^2\tilde{T}_2(\xi, y) + A^3\tilde{T}_3(\xi, y) + \ldots \quad (24b)$$

Substitution of these expansions in equations (20), (22) and (23) would yield a sequence of boundary value problems for $\tilde{\psi}_i$ and $\tilde{T}_i (i = 0, 1, 2, 3, \ldots)$. Let us first consider the problem for $\tilde{T}_0$. We have

$$\nabla^2\tilde{T}_0 = 0 \quad (25a)$$

with

$$\tilde{T}_0(0, y) = 1, \quad \tilde{T}_{0y}(\xi, 0) = \tilde{T}_{0y}(\xi, -1) = 0 \quad (25b\text{–}d)$$

$$\lim_{\xi\to\infty} \tilde{T}_0 = \frac{1}{2}(1 + C_0). \quad (25e)$$

Condition (25e) is obtained by matching the inner and outer solutions (24b) and (15b), for temperature, to leading order. Clearly problem (25) has the unique solution $\tilde{T}_0 = 1$, and as a result, we must have

$$C_0 = 1. \quad (26)$$

The problem for $\tilde{T}_1$ is given by

$$\nabla^2\tilde{T}_1 = 0 \quad (27a)$$

$$\tilde{T}_1(0, y) = 0, \quad \tilde{T}_{1y}(\xi, 0) = \tilde{T}_{1y}(\xi, -1) = 0 \quad (27b\text{–}d)$$

$$\lim_{\xi\to\infty} \tilde{T}_1 = \frac{1}{2}C_1 - \xi. \quad (27e)$$

Condition (27e) follows from matching two terms of the inner and outer expansions for temperature. The only solution for $\tilde{T}_1$ is $\tilde{T}_1 = -\xi$ so that

$$C_1 = 0. \quad (28)$$

With $\tilde{T}_0$ and $\tilde{T}_1$ known, the problem for $\tilde{\psi}_0$ can be formulated as

$$\nabla^4\tilde{\psi}_0 - \sigma^2\nabla^2\tilde{\psi}_0 = -\sigma^2 \quad (29a)$$

$$\tilde{\psi}_0(0, y) = \tilde{\psi}_{0\xi}(0, y) = 0 \quad (29b,c)$$

$$\tilde{\psi}_0(\xi, 0) = \tilde{\psi}_{0y}(\xi, 0) = 0 \quad (29d,e)$$

$$\tilde{\psi}_0(\xi, -1) = \tilde{\psi}_{0y}(\xi, -1) = 0. \quad (29f,g)$$

The matching conditions for $\tilde{\psi}_0$ are obtained by matching the inner and outer solutions for ψ, to leading order. These are

$$\lim_{\xi\to\infty} \tilde{\psi}_0 = A^* e^{\sigma y} + B^* e^{-\sigma y} + \frac{1}{2}y^2 + C^* y + D^* \quad (30a)$$

$$\lim_{\xi\to\infty} \tilde{\psi}_{0\xi} = 0. \quad (30b)$$

The problem consisting of equations (29) and (30) is solved numerically for a few selected values of the Darcy parameter, σ. The computed streamlines are plotted in Figs. 2–4 for $\sigma = 10, 20$ and 70, respectively. The figures show that the streamlines become almost parallel for $\xi \geq 2$. This is to be expected since the horizontal length scale characterizing the flow near the sidewalls is comparable to the aspect ratio of the cavity. It is clear from these figures that as σ increases, i.e. Da decreases, the streamlines move closer to the solid boundaries, displaying the emergence of a boundary layer structure. Observe, for instance, how the streamline given by $\psi = -7.4 \times 10^{-2}$ moves closer and closer to the solid boundaries as the value of σ increases from 10 to 70. The leading order core velocity profile is drawn in Fig. 5 which also depicts the boundary layer behavior when σ becomes large. Note that Darcy's law permits a slip velocity at the upper (and lower) surface of the cavity and therefore the maximum horizontal velocity in the core occurs at this boundary. With the present (Brinkman) model, on the other hand, a no-slip boundary condition can be imposed at the upper (and lower) surface. As a result, the maximum horizontal velocity is reached at an interior point along the vertical, as seen in Fig. 5. Furthermore, the figure shows that the location of this maximum moves toward the upper (and lower) boundary as σ increases, i.e. Da decreases, finally approaching the surface in the limit $Da \to 0$.

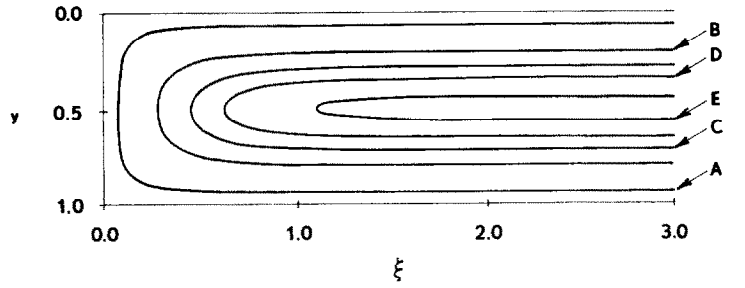

FIG. 2. Leading order streamlines in the boundary layer region near the hot sidewall for $\sigma = 10$ (case I): $A = -2.2 \times 10^{-2}$, $B = -3.8 \times 10^{-2}$, $C = -5.5 \times 10^{-2}$, $D = -6.5 \times 10^{-2}$, $E = -7.4 \times 10^{-2}$.

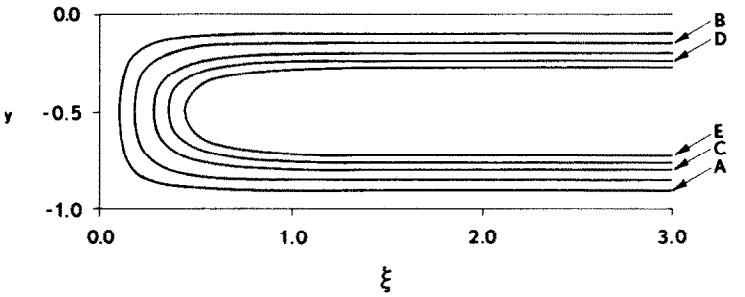

FIG. 3. Leading order streamlines in the boundary layer region near the hot sidewall for $\sigma = 20$ (case I). (Same legend as in Fig. 2.)

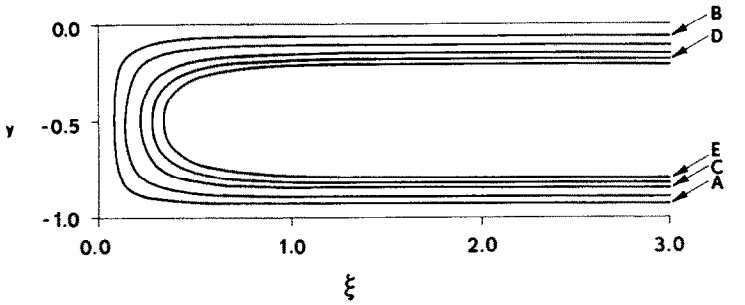

FIG. 4. Leading order streamlines in the boundary layer region near the hot sidewall for $\sigma = 70$ (case I). (Same legend as in Fig. 2.)

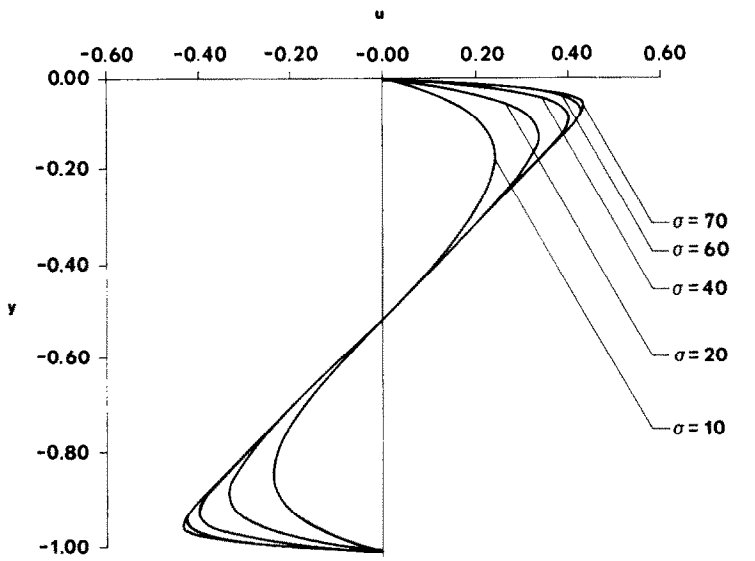

FIG. 5. Core velocity profiles for selected values of σ for a cavity with all rigid boundaries (case I).

Next we examine the problem for the temperature perturbation $\tilde{T}_2$. Introducing a scaled temperature variable $\tilde{T}_2' = \tilde{T}_2/Ra$, we have

$$\nabla^2 \tilde{T}_2' = -\tilde{\psi}_{0y} \tag{31a}$$

$$\tilde{T}_2'(0, y) = 0, \quad \tilde{T}_{2y}'(\xi, 0) = \tilde{T}_{2y}'(\xi, -1) = 0 \tag{31b,c}$$

$$\lim_{\xi \to \infty} \tilde{T}_2' = \frac{1}{2} C_2' + [f(-1/2) - f(y)] \tag{31d}$$

where

$$f(y) = \frac{A^*}{\sigma} e^{\sigma y} - \frac{B^*}{\sigma} e^{-\sigma y} + \frac{1}{6} y^3 + \frac{C^*}{2} y^2 + D^* y \tag{31e}$$

and $C_2' = C_2/Ra$. The solution for $\tilde{T}_2'$ is to be found numerically. However, it is possible to determine C_2' without actually solving for $\tilde{T}_2'$. This can be done as follows. Defining

$$w(\xi) = \int_{-1}^{0} \tilde{T}_2'(\xi, y)\, dy \tag{32}$$

and noting that

$$\int_{-1}^{0} [f(-1/2) - f(y)]\, dy = 0 \tag{33}$$

we find

$$d^2 w/d\xi^2 = 0, \quad w(0) = 0, \quad \lim_{\xi \to \infty} w(\xi) = \frac{1}{2} C_2'. \tag{34}$$

Clearly the only solution is $w = 0$ and therefore $C_2' = 0$. A numerical solution for $\tilde{T}_2'$ is also obtained. This numerical solution will be needed in the computation of $\tilde{T}_3$ and hence the constant C_3.

We are now in a position to formulate the problem for $\tilde{\psi}_1$. Writing

$$\tilde{\psi}_1 = Ra\, \tilde{\psi}_1' + Gr\, \tilde{\psi}_1'' \tag{35}$$

we obtain the equations

$$\nabla^2 \tilde{\psi}_1' - \sigma^2 \nabla^2 \tilde{\psi}_1' = \sigma^2 \tilde{T}_{2\xi}' \tag{36a}$$

$$\nabla^4 \tilde{\psi}_1'' - \sigma^2 \nabla^2 \tilde{\psi}_1'' = \sigma^2 [\tilde{\psi}_{0y}(\tilde{\psi}_{0\xi yy} + \tilde{\psi}_{0\xi\xi\xi}) - \tilde{\psi}_{0\xi}(\tilde{\psi}_{0yyy} + \tilde{\psi}_{0\xi\xi y})] \tag{36b}$$

which are to be solved subject to the homogeneous boundary conditions (29b)–(29g) with $\tilde{\psi}_0$ replaced by $\tilde{\psi}_1'$ and $\tilde{\psi}_1''$, respectively, and the following matching conditions

$$\lim_{\xi \to \infty} \tilde{\psi}_1' = \lim_{\xi \to \infty} \tilde{\psi}_{1\xi}' = 0 \tag{37a}$$

$$\lim_{\xi \to \infty} \tilde{\psi}_1'' = \lim_{\xi \to \infty} \tilde{\psi}_{1\xi}'' = 0. \tag{37b}$$

Again, the solution for $\tilde{\psi}_1'$ and $\tilde{\psi}_1''$ can be obtained via numerical computation. However, as we shall see later, these solutions are not needed in calculating the Nusselt number up to $O(A^3)$, the order to which the present analysis is carried out. For this reason, a numerical solution for $\tilde{\psi}_1'$ or $\tilde{\psi}_1''$ will not be obtained here.

Finally, in order to determine C_3, we consider the problem for $\tilde{T}_3$. Setting

$$\tilde{T}_3 = Ra^2(\tilde{T}_3' + \tilde{T}_3''') + Ra\, Gr\, \tilde{T}_3'' \tag{38a}$$

and

$$C_3 = Ra^2(C_3' + C_3''') + Ra\, Gr\, C_3'' \tag{38b}$$

we find that $\tilde{T}_3'$ satisfies the equation

$$\nabla^2 \tilde{T}_3' = \tilde{\psi}_{0y} \tilde{T}_{2\xi}' - \tilde{\psi}_{0\xi} \tilde{T}_{2y}' \tag{39a}$$

and the conditions

$$\tilde{T}_3'(0, y) = 0, \quad \tilde{T}_{3y}'(\xi, 0) = \tilde{T}_{3y}'(\xi, -1) = 0 \tag{39b–d}$$

$$\lim_{\xi \to \infty} \tilde{T}_3'(\xi, y) = \frac{1}{2} C_3'. \tag{39e}$$

On the other hand, $\tilde{T}_3''$ and $\tilde{T}_3'''$ solve the equations

$$\nabla^2 \tilde{T}_3'' = -\tilde{\psi}_{1y}'', \qquad \nabla^2 \tilde{T}_3''' = -\tilde{\psi}_{1y}'$$

respectively. The boundary and matching conditions for $\tilde{T}_3''$ or $\tilde{T}_3'''$ are the same as conditions (39b)–(39e) with $\tilde{T}_3'$ replaced by $\tilde{T}_3''$ or $\tilde{T}_3'''$ and C_3' by C_3'' or C_3'''. Since both $\tilde{\psi}_1'$ and $\tilde{\psi}_1''$ must vanish at the top and bottom surfaces ($y = 0, -1$) of the cavity, we can show following a procedure similar to the evaluation of C_2' that $C_3'' = C_3''' = 0$. Determination of C_3' however requires a numerical computation of $\tilde{T}_3'$. We solve the problem consisting of equations (39a)–(39d) and the condition

$$\lim_{\xi \to \infty} \tilde{T}_{3\xi}' = 0 \tag{40}$$

instead of condition (39e) and from the numerical solution thus obtained, C_3' is evaluated using the relation

$$C_3' = 2\left[\lim_{\xi \to \infty} \int_{-1}^{0} \tilde{T}_3'(\xi, y)\, dy\right] \tag{41}$$

which follows from an integration of condition (39e) along the vertical. Note that C_3' depends on σ. Numerically computed values of C_3' for several choices of σ are shown in Table 1. The table also contains values of C_3' for case II when the cavity has a free upper surface (see Section 6).

The constant k_1 representing the horizontal temperature gradient in the core region can now be expressed as

$$k_1 = 1 + A^3 Ra^2 C_3' + \ldots. \tag{42}$$

5. THE NUSSELT NUMBER

The net heat transfer rate through the cavity was defined earlier in terms of a Nusselt number, according to equation (14). However, for the present configuration, the Nusselt number can be derived in a different way. Since the upper and lower surfaces of the cavity

are insulated, the heat flux through any vertical section of the cavity must be a constant, equal to the heat transfer rate across the cold sidewall. In view of this, the Nusselt number can be found from the core solution, using the formula

$$Nu = -\int_{-1}^{0} (T_x - Ra\psi_y T)\,dy. \tag{43}$$

Substituting the core solutions (15) for the streamfunction and the temperature in formula (43), it can be shown that

$$Nu = k_1(1 + A^2 Ra^2 k_1^2 M) \tag{44}$$

where the quantity M, depending on σ, has the value

$$M = \int_{-1}^{0} \left(A^* e^{\sigma y} + B^* e^{-\sigma y} + \frac{1}{2}y^2 + C^* y + D^*\right)^2 dy. \tag{45}$$

Inserting expression (42) for k_1 in equation (44), we can write

$$Nu = 1 + A^2 Ra^2(M + C_3' A) + O(A^4). \tag{46}$$

This last equation determines the Nusselt number, correct to $O(A^3)$. It should be emphasized that formula (43) holds for a cavity with all rigid boundaries as well as for a cavity with a free upper surface provided that its horizontal surfaces are thermally insulated.

Evaluation of the intergal in equation (45) gives

$$\begin{aligned} M = {} & \frac{A^{*2}}{2\sigma}(1 - e^{-2\sigma}) + \frac{B^{*2}}{2\sigma}(e^{2\sigma} - 1) \\ & + \frac{1}{3}C^{*2} + D^{*2} + \frac{1}{20} + 2\left[A^*B^* + \frac{A^*}{2}\left\{\frac{2}{\sigma^3}\right.\right. \\ & \left. - \left(\frac{1}{\sigma} + \frac{2}{\sigma^2} + \frac{2}{\sigma^3}\right)e^{-\sigma}\right\} + A^*C^*\left\{\left(\frac{1}{\sigma} + \frac{1}{\sigma^2}\right)e^{-\sigma}\right. \\ & \left. - \frac{1}{\sigma^2}\right\} + \frac{A^*D^*}{\sigma}(1 - e^{-\sigma}) - \frac{B^*}{2}\left\{\frac{2}{\sigma^3} - \left(\frac{1}{\sigma} - \frac{2}{\sigma^2}\right.\right. \\ & \left. + \frac{2}{\sigma^3}\right)e^{\sigma}\right\} - B^*C^*\left\{\frac{1}{\sigma^2} + \left(\frac{1}{\sigma} - \frac{1}{\sigma^2}\right)e^{\sigma}\right\} \\ & + \frac{B^*D^*}{\sigma}(e^{\sigma} - 1) - \frac{C^*D^*}{2} - \frac{C^*}{8} + \frac{D^*}{6}\Bigg]. \end{aligned} \tag{47}$$

For a cavity with all rigid boundaries (case I), this result can be further simplified to

$$\begin{aligned} M = {} & \frac{A^{*2}}{\sigma}(1 + 2\sigma e^{-\sigma} - e^{-2\sigma}) \\ & + D^{*2} - \frac{D^*}{6} - \frac{2}{\sigma^4} + \frac{1}{120}. \end{aligned} \tag{48}$$

In deriving equation (48) from equation (47), we have used the fact that $C^* = 1/2$ and the relation $B^* = A^* e^{-\sigma}$ (see equations (15c) and (15d)).

The Nusselt number for case I can now be computed as follows. Consider a cavity for which the parameters A, σ and Ra are given. First we calculate M using equation (48) with the values of A^* and D^* from equations (15c) and (15f). Next we determine C_3' from Table 1 or by the use of equation (41). Finally we substitute the values of M, C_3', A and Ra in formula (46), yielding the Nusselt number.

6. CAVITY WITH A FREE UPPER SURFACE

In this section we examine case II, i.e. the situation when the upper surface of the cavity is free but thermally insulated. For this case, the dimensionless equations (7d) and (12) and boundary conditions (13) would still apply with the exception that the no-slip condition ($\psi_y = 0$) on the upper surface $y = 0$ (see condition (13c)) should be replaced by the condition $\psi_{yy} = 0$, i.e. we now have

$$y = 0: \qquad \psi = \psi_{yy} = 0, \qquad T_y = 0. \tag{49}$$

Condition (49) reflects the fact that the upper surface of the cavity is free of shear stress. We shall assume that this free surface remains horizontal everywhere.

As in case I, the flow structure in the cavity consists of a parallel core joined by turning flows near the sidewalls. The core solutions may still be given by equations (15) but with

$$A^* = [(\sigma^2 - 2) + 2(1 - \sigma)e^{\sigma}]/(2\sigma D) \tag{50a}$$

$$B^* = -[(\sigma^2 - 2) + 2(1 + \sigma)e^{-\sigma}]/(2\sigma D) \tag{50b}$$

$$C^* = (\sigma^2 \cosh\sigma - 2\sigma \sinh\sigma + 2\cosh\sigma - 2)/D \tag{50c}$$

$$D^* = 1/\sigma^2 \tag{50d}$$

where

$$D = 2\sigma(\sigma \cosh\sigma - \sinh\sigma). \tag{50e}$$

The core velocity profiles for selected values of σ are shown in Fig. 7.

An expression for the Nusselt number for the present case can be derived in the form of equation (44) where the constant k_1 represents the core temperature gradient, as before. Recall that for the cavity with all rigid boundaries (case I), constants k_1 and k_2 (see equation (17)) are related by the centro-symmetry condition (16). In other words, it was possible to suppress k_2 in favor of k_1. As a result, it was sufficient to analyze the boundary layer flow near one of the sidewalls, e.g. the hot sidewall only. Due to lack of symmetry in the present problem, k_2 cannot be eliminated in an obvious way. Therefore, it will, in general, be necessary to examine the boundary layers

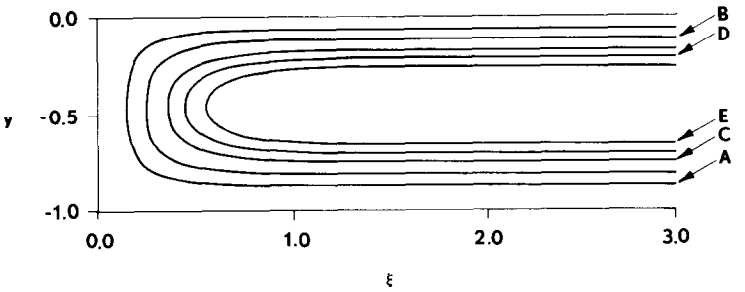

FIG. 6. Leading order streamlines in the boundary layer region near the hot sidewall for $\sigma = 10$ (case II). (Same legend as in Fig. 2.)

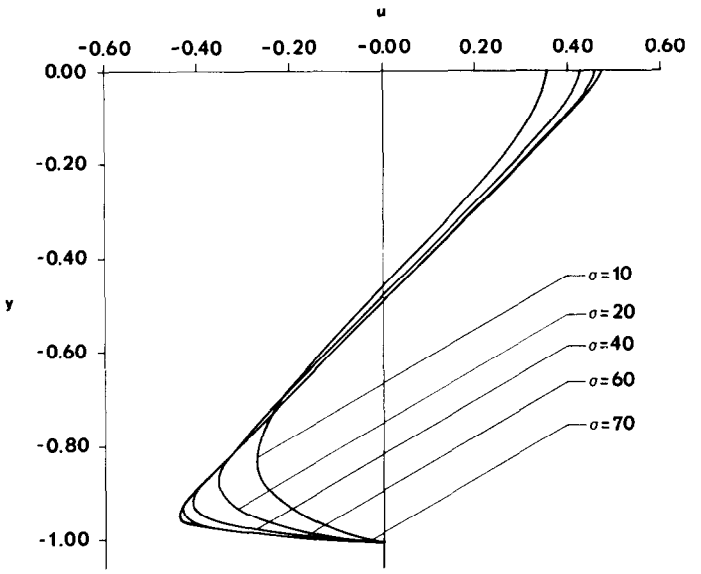

FIG. 7. Core velocity profiles for selected values of σ for a cavity with a free upper surface (case II).

near both sidewalls, in order to determine k_1. It is convenient to expand k_2 in the form

$$k_2 = \bar{C}_0 + \bar{C}_1 A + \bar{C}_2 A^2 + \bar{C}_3 A^3 + \ldots \quad (51)$$

analogous to equation (18). We shall see that although there is no apparent symmetry in this problem, the boundary layer equations near the hot and cold sidewalls exhibit certain symmetries, leading to considerable simplification. The details of the boundary layer solutions are given in the Appendix. The aim of these calculations is to determine the constants C_0, C_1, C_2 and C_3 appearing in expression (18) for k_1. We find that

$$C_0 = 1,\ C_1 = C_2 = 0 \text{ and } C_3 = Ra^2 C_3' \quad (52a\text{–}c)$$

where the values of C_3' are obtained from a numerical solution of T_3' (see Appendix) near the hot sidewall. These are listed in Table 1 for selected values of σ. The core temperature gradient k_1 is still given by expression (42). Accordingly the Nusselt number up to $O(A^3)$ can be computed from equation (46). Note however that M now has the value given in equation (47) with A^*, B^*, C^* and D^* defined by equations (50).

7. RESULTS AND DISCUSSION

As mentioned earlier, the main objective of this work is to determine the rate of heat transfer through the cavity for cases I and II and to estimate the effect of a free upper surface on the heat transfer rate.

It is evident from Figs. 5 and 7 that for the same value of σ, the magnitude of the core velocity in case II is higher than that in case I. This is due to the fact that the condition of zero shear at the free surface allows larger horizontal velocities within the cavity. The increased core velocity for the free surface problem leads to a smaller horizontal temperature gradient in the core, resulting in an enhancement of the longitudinal convective transport of heat. Accordingly, we shall find that for a given value of σ and Ra, the Nusselt number for case II is larger than that for case I.

For the purpose of presenting the heat transfer results, we consider a cavity of aspect ratio 0.1 with Rayleigh number in the range 10–100 and the Darcy parameter σ between 4 and 70. This range of σ corresponds to Darcy numbers (Da) between 6.25×10^{-2} and 2.04×10^{-4}. With the values of σ and C_3' shown in Table 1, the Nusselt numbers are

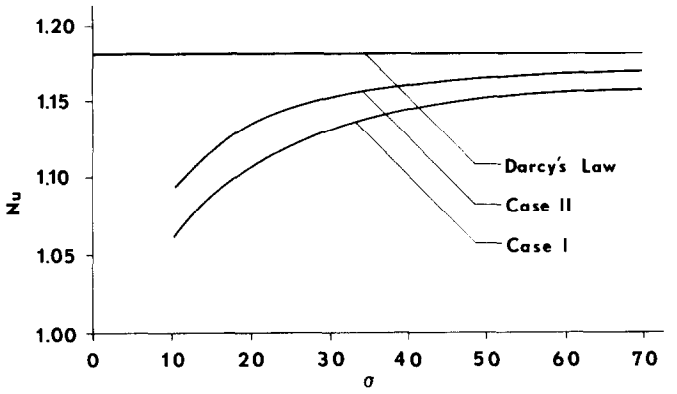

FIG. 8. Comparison of Brinkman (present) and Darcy models for a cavity of aspect ratio 0.1, with $Ra = 50$.

Table 1. Numerically computed values of C_3' for various values of σ in cases I and II

σ	Cavity with all rigid boundaries (case I)	Cavity with a free upper surface (case II)
4	-4.402×10^{-6}	-9.200×10^{-4}
5	-2.800×10^{-5}	-1.763×10^{-3}
6	-1.140×10^{-4}	-2.565×10^{-3}
8	-1.022×10^{-3}	-3.895×10^{-3}
10	-1.884×10^{-3}	-4.860×10^{-3}
20	-4.543×10^{-3}	-7.042×10^{-3}
30	-5.742×10^{-3}	-7.792×10^{-3}
40	-6.404×10^{-3}	-8.164×10^{-3}
50	-6.826×10^{-3}	-8.388×10^{-3}
60	-7.110×10^{-3}	-8.539×10^{-3}
70	-7.328×10^{-3}	-8.644×10^{-3}

computed from equation (46) for a cavity with all rigid boundaries (case I) and a cavity with a free upper surface (case II). Using these results we have plotted in Fig. 8 the variation of the Nusselt number with σ for a typical value of $Ra = 50$. In the same figure, the Nusselt number obtained from a numerical calculation using Darcy's law is also shown by a horizontal line. The Darcy results are taken from the work of Hickox and Gartling [19]. It is clear from Fig. 8 that with Ra fixed, the Nusselt number increases as σ increases (i.e. Da decreases) for both cases I and II. When σ is large, the curves for cases I and II are seen to approach the Darcy value as an asymptote. This is to be expected since in the limit $\sigma \to \infty$, the present (Brinkman) model reduces to the Darcy model. Furthermore, it is apparent that for the same Rayleigh number, the curve for case II lies above the curve for case I indicating that the heat transfer rate for a cavity with a free upper surface is higher than that for a cavity with all rigid boundaries.

Table 2 shows the values of Nu for $\sigma = 70$ and $Ra = 25$, 50 and 100 for both cases I and II. For comparison we have included in this table the Nusselt numbers obtained by Hickox and Gartling [19], Walker and Homsy [20] and Bejan and Tien [21] using Darcy's law. The calculations reported in refs. [20, 21] are based on an asymptotic approach in the limit of vanishingly small aspect ratio. It should also be pointed out that the results in ref. [21] are correct to $O(A^6)$.

Enhancement in heat transfer due to the presence of a free upper surface can also be seen from Tables 3–6 where we have presented the Nusselt numbers for various values of Ra with $\sigma = 10$, 20, 40 and 70, respectively. The numerical values in these tables clearly indicate that for both cases I and II, the Nusselt number increases as σ increases for the same value of Ra. In addition, the Nusselt number increases for both cases as Ra increases with σ fixed. This trend is also clear from formula (46). With a given set of σ and Ra, we see that the Nusselt number for a cavity with a free upper surface is always greater than that for a cavity with all rigid boundaries. The maximum percentage increase in the heat transfer rate in case II compared to case I can be estimated to be 11.5%. This occurs when $\sigma = 10$ and $Ra = 100$ (see Table 3), for a cavity of aspect ratio 0.1. From these results we conclude that for the range of parameters considered, presence of a free surface may significantly increase the heat transfer rate through the cavity, especially when the permeability of the medium is large. We also find that with a fixed value of Ra, the percent increase in the Nusselt number decreases as σ increases. Finally, our computations reveal that the Brinkman model and Darcy's law give virtually the same result for the Nusselt number when the Darcy number, based on the depth of the cavity, is less than the order of 10^{-4}.

Table 2. Comparison of Nusselt number results based on the present study (Brinkman model) and Darcy's law

Ra	Present study ($\sigma = 70$) Case I	Present study ($\sigma = 70$) Case II	Hickox and Gartling [19]	Walker and Homsy [20]	Bejan and Tien [21]
25	1.04038	1.04292	1.046	1.04587	1.04142
50	1.16154	1.17167	1.182	1.18349	1.16240
100	1.64617	1.68667	1.690	1.73396	1.60565

Table 3. Nusselt numbers for various values of Ra with $\sigma = 10$

Ra	Cavity with all rigid boundaries (case I) Nu_{I}	Cavity with a free upper surface (case II) Nu_{II}	Percent increase $\frac{Nu_{\mathrm{II}} - Nu_{\mathrm{I}}}{Nu_{\mathrm{I}}} \times 100\%$
10	1.00236	1.00378	0.142
20	1.00945	1.01510	0.560
30	1.02125	1.03398	1.246
40	1.03778	1.06040	2.180
50	1.05904	1.09438	3.337
60	1.08502	1.13591	4.690
70	1.11572	1.18494	6.204
80	1.15114	1.24149	7.849
90	1.19128	1.30556	9.593
100	1.23615	1.37803	11.477

Table 4. Nusselt numbers for various values of Ra with $\sigma = 20$

Ra	Cavity with all rigid boundaries (case I) Nu_{I}	Cavity with a free upper surface (case II) Nu_{II}	Percent increase $\frac{Nu_{\mathrm{II}} - Nu_{\mathrm{I}}}{Nu_{\mathrm{I}}} \times 100\%$
10	1.00436	1.00551	0.114
20	1.01742	1.02203	0.453
30	1.03921	1.04956	0.996
40	1.06970	1.08811	1.721
50	1.10890	1.13767	2.594
60	1.15682	1.19824	3.580
70	1.21345	1.26983	4.646
80	1.27879	1.35243	5.758
90	1.35285	1.44604	6.888
100	1.43561	1.55067	8.015

Table 5. Nusselt numbers for various values of Ra with $\sigma = 40$

Ra	Cavity with all rigid boundaries (case I) Nu_{I}	Cavity with a free upper surface (case II) Nu_{II}	Percent increase $\frac{Nu_{\mathrm{II}} - Nu_{\mathrm{I}}}{Nu_{\mathrm{I}}} \times 100\%$
10	1.00577	1.00646	0.068
20	1.02308	1.02583	0.269
30	1.05192	1.05812	0.589
40	1.09230	1.10332	1.008
50	1.14422	1.16143	1.504
60	1.20768	1.23246	2.052
70	1.28268	1.31641	2.629
80	1.36921	1.41326	3.217
90	1.46729	1.52304	3.799
100	1.57690	1.64573	4.365

Table 6. Nusselt numbers for various values of Ra with $\sigma = 70$

Ra	Cavity with all rigid boundaries (case I) Nu_{I}	Cavity with a free upper surface (case II) Nu_{II}	Percent increase $\frac{Nu_{\mathrm{II}} - Nu_{\mathrm{I}}}{Nu_{\mathrm{I}}} \times 100\%$
10	1.00646	1.00686	0.040
20	1.02585	1.02746	0.157
30	1.05816	1.06178	0.342
40	1.10339	1.10983	0.584
50	1.16154	1.17162	0.868
60	1.23262	1.24713	1.177
70	1.31662	1.33637	1.500
80	1.41356	1.43934	1.824
90	1.52340	1.55604	2.142
100	1.64617	1.68667	2.460

REFERENCES

1. P. Cheng, Heat transfer in geothermal systems, *Adv. Heat Transfer* **14,** 1 (1978).
2. M. A. Combarnous and S. A. Bories, Hydrothermal convection in saturated porous media, *Adv. Hydroscience* **10,** 231 (1975).
3. A. O. O. Denloye and J. S. M. Botterill, Heat transfer in flowing packed beds, *Chem. Engng Sci.* **32,** 461 (1977).
4. A. Bejan, Lateral intrusion of natural convection into a horizontal porous structure, *J. Heat Transfer* **103,** 237 (1981).
5. G. S. Beavers and D. D. Joseph, Boundary conditions at a naturally permeable wall, *J. Fluid Mech.* **30,** 197 (1967).
6. P. G. Saffman, On the boundary conditions at the free surface of a porous medium, *Stud. appl. Math.* **2,** 93 (1971).
7. H. C. Brinkman, A calculation of the viscous force exerted by a flowing fluid on a dense swarm of particles, *Appl. scient Res.* **A1,** 81 (1948).
8. C. K. W. Tam, The drag on a cloud of spherical particles in a low Reynolds number flow, *J. Fluid Mech.* **38,** 537 (1969).
9. T. S. Lundgren, Slow flow through stationary random beds and suspensions of spheres, *J. Fluid Mech.* **51,** 273 (1972).
10. J. Koplik, H. Levine and A. Zee, Viscosity renormalization in the Brinkman equation, *Physics Fluids* **26,** 2864 (1983).
11. I. D. Howells, Drag due to the motion of a Newtonian fluid through a sparse random array of small fixed rigid objects, *J. Fluid Mech.* **64,** 449 (1974).
12. E. J. Hinch, An averaged equation approach to particle interactions in a fluid suspension, *J. Fluid Mech.* **83,** 695 (1977).
13. B. K. C. Chan, C. M. Ivey and J. M. Barry, Natural convection in enclosed porous media with rectangular boundaries, *J. Heat Transfer* **92,** 21 (1970).
14. N. Rudraiah, B. Veerappa and S. B. Rao, Effects of nonuniform thermal gradient and adiabatic boundaries on convection in porous media, *J. Heat Transfer* **102,** 254 (1980).
15. K. Nandakumar and J. H. Masliyah, Laminar flow past a permeable sphere, *Can. J. chem. Engng* **60,** 202 (1982).
16. S. Haber and R. Mauri, Boundary conditions for Darcy's flow through porous media, *Int. J. multiphase flow* **9,** 561 (1983).
17. T. W. Tong and E. Subramanian, A boundary-layer analysis for natural convection in vertical porous enclosures—use of the Brinkman-extended Darcy model, *Int. J. Heat Mass Transfer* **28,** 563 (1985).
18. A. Bejan, *Convection Heat Transfer.* Wiley, New York (1984).
19. C. E. Hickox and D. K. Gartling, A numerical study of natural convection in a horizontal porous layer subjected to an end-to-end temperature difference, *J. Heat Transfer* **103,** 797 (1981).
20. K. L. Walker and G. M. Homsy, Convection in a porous cavity, *J. Fluid Mech.* **87,** 449 (1978).
21. A. Bejan and C. L. Tien, Natural convection in a horizontal porous medium subjected to an end-to-end temperature difference, *J. Heat Transfer* **100,** 191 (1978).
22. M. Muskat, *The Flow of Homogeneous Fluids through Porous Media.* Edwards, Michigan (1946).
23. S. Whitaker, Advances in the theory of fluid motion in porous media, *Ind. Engng Chem.* **61,** 110 (1969).
24. J. C. Slattery, Multiphase viscoelastic flow through porous media, *A.I.Ch.E Jl* **14,** 50 (1968).
25. K. Vafai and C. L. Tien, Boundary and inertia effects of flow and heat transfer in porous media, *Int. J. Heat Mass Transfer* **24,** 195 (1981).
26. D. E. Cormack, L. G. Leal and J. Imberger, Natural convection in a shallow cavity with differentially heated end walls. Part I. Asymptotic theory, *J. Fluid Mech.* **65,** 209 (1974).

APPENDIX

Boundary layer analysis for the cavity with a free upper surface

By setting $x = A\xi$, the flow in the hot boundary layer region in this case can be described by equations (20) subject to the following boundary conditions

$$\xi = 0: \quad \psi = \psi_\xi = 0, \quad T = 1; \tag{A1}$$

$$y = 0: \quad \psi = \psi_{yy} = 0, \quad T_y = 0; \tag{A2}$$

$$y = -1: \quad \psi = \psi_y = 0, \quad T_y = 0. \tag{A3}$$

The matching conditions (23) may still be used with the core solutions identified by equations (15) where the constants A^*, B^*, C^* and D^* are now given by equations (50). The streamfunction and the temperature are expanded in the form of expansions (24), as usual. Substituting these expansions into equations (20), boundary conditions (A1)–(A3) and matching conditions (23), we find, to a leading approximation, the problems

$$\nabla^2 \bar{T}_0 = 0, \quad \bar{T}_0(0, y) = 1,$$
$$\bar{T}_{0y}(\xi, 0) = \bar{T}_{0y}(\xi, -1) = 0, \quad \lim_{\xi \to \infty} \bar{T}_0 = \bar{C}_0 \tag{A4}$$

and

$$\nabla^4 \bar{\psi}_0 - \sigma^2 \nabla^2 \bar{\psi}_0 = \sigma^2 \bar{T}_{1\xi},$$
$$\bar{\psi}_0(0, y) = \bar{\psi}_{0\xi}(0, y) = 0,$$
$$\bar{\psi}_0(\xi, 0) = \bar{\psi}_{0yy}(\xi, 0) = 0,$$
$$\bar{\psi}_0(\xi, -1) = \bar{\psi}_{0y}(\xi, -1) = 0, \tag{A5}$$

$$\lim_{\xi \to \infty} \bar{\psi}_0 = A^* e^{\sigma y} + B^* e^{-\sigma y} + \frac{1}{2} y^2 + C^* y + D^*,$$

$$\lim_{\xi \to \infty} \bar{\psi}_{0\xi} = 0.$$

At the next three orders, we have the following problems for temperature

$$\nabla^2 \bar{T}_1 = 0, \quad \bar{T}_1(0, y) = \bar{T}_{1y}(\xi, 0) = \bar{T}_{1y}(\xi, -1) = 0,$$
$$\lim_{\xi \to \infty} \bar{T}_1 = \bar{C}_1 - C_0 \xi \tag{A6}$$

$$\nabla^2 \bar{T}_2 = -Ra\, \bar{\psi}_{0y}, \quad \bar{T}_2(0, y) = \bar{T}_{2y}(\xi, 0) = \bar{T}_{2y}(\xi, -1) = 0$$
$$\lim_{\xi \to \infty} \bar{T}_2 = \bar{C}_2 - C_1 \xi - Ra\, C_0^2 g(y) \tag{A7}$$

where

$$g(y) = \frac{A^*}{\sigma} e^{\sigma y} - \frac{B^*}{\sigma} e^{-\sigma y} + \frac{1}{6} y^3 + \frac{C^*}{2} y^2 + D^* y \tag{A8}$$

$$\nabla^2 \bar{T}_3 = Ra[\bar{\psi}_{1y} \bar{T}_{1\xi} + (\bar{\psi}_{0y} \bar{T}_{2\xi} - \bar{\psi}_{0\xi} \bar{T}_{2y})],$$
$$\bar{T}_3(0, y) = \bar{T}_{3y}(\xi, 0) = \bar{T}_{3y}(\xi, -1) = 0, \tag{A9}$$
$$\lim_{\xi \to \infty} \bar{T}_3 = \bar{C}_3 - C_2 \xi - 2Ra\, C_0 C_1 g(y).$$

Our aim here is to determine the constants C_0 through C_3 in expansion (18) for k_1 and calculate the Nusselt number using equation (44). It can be shown, analogous to the cavity with all rigid boundaries, that the problems for $\bar{\psi}_1$ and the higher approximations of ψ are not needed in the computation of these constants. Therefore we shall not write down these problems explicitly.

Near the cold sidewall, we let $x = 1 - A\eta$ and write expansions (24) with ξ replaced by η and a caret placed over the functions ψ_i and T_i (instead of a tilde) to distinguish them from the corresponding expansions in the hot boundary layer. It follows that the problems for temperature in this boundary layer are given by

$$\nabla^2\hat{T}_0 = 0, \quad \hat{T}_0(0, y) = \hat{T}_{0y}(\eta, 0) = \hat{T}_{0y}(\eta, -1) = 0, \quad \lim_{\xi\to\infty} \hat{T}_0 = \bar{C}_0 - C_0; \tag{A10}$$

$$\nabla^2\hat{T}_1 = 0, \quad \hat{T}_1(0, y) = \hat{T}_{1y}(\eta, 0) = \hat{T}_{1y}(\eta, -1) = 0, \quad \lim_{\eta\to\infty} \hat{T}_1 = (\bar{C}_1 - C_1) + C_0\eta; \tag{A11}$$

$$\nabla^2\hat{T}_2 = -Ra\,\hat{\psi}_{0y}, \quad \hat{T}_2(0, y) = \hat{T}_{2y}(\eta, 0) = \hat{T}_{2y}(\eta, -1) = 0, \quad \lim_{\eta\to\infty} \hat{T}_2 = (\bar{C}_2 - C_2) + C_1\eta - Ra\,C_0^2 g(y); \tag{A12}$$

$$\nabla^2\hat{T}_3 = -Ra[\hat{\psi}_{1y}\hat{T}_{1\eta} + (\hat{\psi}_{0y}\hat{T}_{2\eta} - \hat{\psi}_{0\eta}\hat{T}_{2y})], \quad \hat{T}_3(0, y) = \hat{T}_{3y}(\eta, 0) = \hat{T}_{3y}(\eta, -1) = 0, \quad \lim_{\eta\to\infty} \hat{T}_3 = (\bar{C}_3 - C_3) + C_2\eta - 2Ra\,C_0C_1 g(y). \tag{A13}$$

Note that the Laplacian ∇^2 now has the definition (21) with ξ replaced by η.

Consider first problem (A4) for $\bar{T}_0$ which has the only solution $\bar{T}_0(\xi, y) = 1$ so that $\bar{C}_0 = 1$. Similarly the only solution of problem (A10) is $\hat{T}_0(\eta, y) = 0$ and therefore $C_0 = \bar{C}_0 = 1$. By considering problems (A6) and (A11) successively, it is easy to show that $\bar{T}_1(\xi, y) = -\xi$, $\hat{T}_1(\eta, y) = \eta$ and consequently $\bar{C}_1 = C_1 = 0$. Next a numerical solution for $\bar{\psi}_0(\xi, y)$ is found by solving problem (A5). The computed streamlines are shown in Fig. 6 for $\sigma = 10$. The figure clearly exhibits the lack of symmetry in the vertical direction which is caused by the zero-shear condition at the upper surface. It can be easily shown that the problem for the leading order streamfunction in the cold boundary layer, $\hat{\psi}_0(\eta, y)$, becomes identical to that of $\bar{\psi}_0(\xi, y)$ if η is exchanged with ξ and carets replace tildes. Therefore there is no need to examine the problem for $\hat{\psi}_0$.

The constant $\bar{C}_2$ can be determined by analyzing problem (A7). If we define $\bar{T}_2 = Ra\,\bar{T}_2'$ and $\bar{C}_2 = Ra\,\bar{C}_2'$, we obtain conditions (31) with condition (31d) replaced by the condition

$$\lim_{\xi\to\infty} \bar{T}_2' = \bar{C}_2' - g(y). \tag{A14}$$

Then following a procedure similar to that used in Section 4, it can be easily deduced that

$$\bar{C}_2' = \int_{-1}^{0} g(y)\,dy = C^*\left(\frac{1}{6} - \frac{1}{\sigma^2}\right) - \frac{1}{24}. \tag{A15}$$

Similarly by analyzing problem (A12), we can show that $C_2 = 0$. With $\bar{C}_2'$ known, the problem given by conditions (31a)–(31c) and (A14) is solved numerically for $\bar{T}_2'$. The numerical solutions of $\bar{\psi}_0$ and $\bar{T}_2$ will be used to find the solution for $\bar{T}_3$ and thereby determine the constant C_3. We now turn to the problems for $\bar{T}_3$ and $\hat{T}_3$.

It is convenient to write $\bar{T}_3 = Ra^2(\bar{T}_3' + \bar{T}_3''') + Ra\,Gr\,\bar{T}_3''$ and $\bar{C}_3 = Ra^2(\bar{C}_3' + \bar{C}_3''') + Ra\,Gr\,\bar{C}_3''$, analogous to equation (38). We then find that $\bar{T}_3'(\xi, y)$ solves the problem given by conditions (39) with condition (39e) replaced by the condition

$$\lim_{\xi\to\infty} \bar{T}_3'(\xi, y) = \bar{C}_3'. \tag{A16}$$

We shall not write down the problems for $\bar{T}_3''$ or $\bar{T}_3'''$, from which it can be shown that $\bar{C}_3'' = \bar{C}_3''' = 0$. To determine $\bar{C}_3'$, we first solve the $\bar{T}_3'$ problem numerically with requirement (40) instead of condition (A16). Then $\bar{C}_3'$ is found by using the relation

$$\bar{C}_3' = \lim_{\xi\to\infty} \int_{-1}^{0} \bar{T}_3'(\xi, y)\,dy. \tag{A17}$$

Finally to determine C_3, we examine the problem for $\hat{T}_3(\xi, y)$. Set $\hat{T}_3 = Ra^2(\hat{T}_3' + \hat{T}_3''') + Ra\,Gr\,\hat{T}_3''$ and $C_3 = Ra^2(C_3' + C_3''') + Ra\,Gr\,C_3''$ in conditions (A13) to obtain

$$\nabla^2\hat{T}_3' = -(\hat{\psi}_{0y}\hat{T}_{2\eta}' - \hat{\psi}_{0\eta}\hat{T}_{2y}') \tag{A18a}$$

$$\hat{T}_3'(0, y) = \hat{T}_{3y}'(\eta, 0) = \hat{T}_{3y}'(\eta, -1) = 0 \tag{A18b}$$

$$\lim_{\xi\to\infty} \hat{T}_3' = \bar{C}_3' - C_3'. \tag{A18c}$$

Considering problem (A18) above with condition (A18c) replaced by the condition

$$\lim_{\xi\to\infty} \hat{T}_{3\eta}' = 0 \tag{A19}$$

we find that the problems for $\hat{T}_3'(\eta, y)$ and $-\bar{T}_3'(\xi, y)$ are identical. In view of this, we may deduce from conditions (A16) and (A18c) that $C_3' = 2\bar{C}_3'$, from which C_3' can be computed. The remaining constants in C_3, namely C_3'' and C_3''' can be shown to be zero by examining the problems for $\hat{T}_3''$ and $\hat{T}_3'''$. Therefore we have $C_3 = Ra^2C_3'$. This completes the determination of the constants C_0, C_1, C_2 and C_3 (see equations (52)).

CONVECTION NATURELLE DANS UNE CAVITE POREUSE ETROITE—LE MODELE DE BRINKMAN

Résumé—On étudie à l'aide du modèle de Brinkman la convection naturelle dans une cavité poreuse, rectangulaire et étroite avec des parois latérales différemment chauffées. Le transfert thermique à travers la cavité est déterminé en fonction du nombre de Nusselt, dans la limite d'un rapport de forme extrêmement petit. On considère deux types de conditions aux limites. Le cas I concerne une cavité avec toutes les frontières rigides de telle façon que les conditions aux limites d'adhérence soient imposées. Dans le cas II, la cavité a une surface supérieure libre. L'analyse montre que le modèle de Brinkman et la loi de Darcy donnent virtuellement le même résultat, pour le transfert de chaleur, quand le nombre de Darcy basé sur la profondeur de la cavité est inférieur à 10^{-4}. On trouve aussi que la présence d'une surface libre peut augmenter le transfert thermique, particulièrement quand la perméabilité du milieu est forte.

NATÜRLICHE KONVEKTION IN EINEM FLACHEN PORÖSEN HOHLRAUM—DAS BRINKMAN-MODELL

Zusammenfassung—Die natürliche Konvektion in einem flachen, porösen, rechteckigen Hohlraum mit unterschiedlich beheizten Seitenwänden wird mit Hilfe des Brinkman-Modells untersucht. Der Wärmetransport durch den Hohlraum wird für den Fall eines verschwindend kleinen Seitenverhältnisses mit einer Nusselt-Zahl dargestellt. Zwei Arten von Randbedingungen werden untersucht: Im ersten Fall wird ein vollkommener Hohlraum mit Wänden ringsum betrachtet, bei dem die Haftbedingung an den Wänden gilt. Im zweiten Fall hat der Hohlraum eine freie Oberfläche. Die Untersuchung zeigt, daß das Brinkman-Modell und Darcy's Gesetz praktisch dieselben Ergebnisse für den Warmetransport liefern, wenn die Darcy-Zahl, auf die Tiefe des Hohlraums bezogen, kleiner als etwa 10^{-4} ist. Bei Vorhandensein einer freien Oberfläche erhöht sich der Wärmetransport durch den Hohlraum beträchtlich, vor allem, wenn die Permeabilität des porösen Mediums groß ist.

ЕСТЕСТВЕННАЯ КОНВЕКЦИЯ В ТОНКОЙ ПОРИСТОЙ ПОЛОСТИ—МОДЕЛЬ БРИНКМАНА

Аннотация—Естественная конвекция в тонкой пористой прямоугольной полости с неодинаково нагреваемыми боковыми стенками исследуется с помощью модели Бринкмана. Интенсивность теплопереноса через полость определяется с помощью числа Нуссельта для предельно малого отношения высоты к ширине. Рассматриваются два типа граничных условий. В первом случае изучается полость, имеющая все твердые границы, так что на границах отсутствует проскальзывание Во втором случае полость имеет свободную верхнюю поверхность. Анализ показывает, что модель Бринкмана и закон Дарси дают практически одинаковый результат для интенсивности теплопереноса в том случае, когда число Дарси, основанное на глубине полости, меньше 10^{-4}. Также найдено, что свободная поверхность может существенно увеличить интенсивность теплопереноса через полость, особенно когда проницаемость среды велика.